Indian Journal of Chemistry
Vol. 64, June 2025, pp. 598-613
DOI: 10.56042/ijc.v64i6.15749

Hydroxyurea, thiourea, and urea derivatives of coumarins: synthesis, characterization, molecular docking, DFT calculations, pharmacokinetics and anticancer potency

Anand Kumar Yadav[a], Manoj Silwal[b], Neeta Singh[a], Achyut Adhikari[a] & Paras Nath Yadav*[a],

[a] Central Department of Chemistry, Tribhuvan University, Kathmandu, Nepal

[b] New Horizon English Boarding Secondary School, Rupandehi, Butwal, Nepal

E-mail: pnyadav219@gmail.com, paras.yadav@tu.edu.np

Received 15 December 2024; accepted (revised) 2 June 2025

The new Schiff bases (SB1-SB7) of hydroxyurea, thiourea, and urea with 3-acetylcoumarins have been synthesized and characterized by elemental analysis, ESI-HRMS, NMR, FT-IR, and UV-Vis spectroscopic techniques. The studied compounds show dose-dependent good-to-moderate anticancer efficacy. The MTT assay has been performed to determine *in vitro* cytotoxicity on human breast cancer (MCF-7) cells. The selective suppression of the MCF-7 cell line has been demonstrated by the synthesized compounds, with IC_{50} (in µg/mL) of SB1 (398.0), SB4 (354.8), SB3 (353.0), SB2 (298.2), SB6 (269.5), SB7 (166.7), and SB5 (157.9). The most potent compound, 1-hydroxy-3-[(1*E*)-1-(4-hydroxy-2-oxo-2*H*-chromen-3-yl)ethylidene]urea, (SB5) shows significant cytotoxicity with an IC_{50} value of 157.9 µg/mL against the tested cell line. The treated compound (SB5) shows a higher proportion of cells in G1 and S phases as (32.53%), and (19.77%) respectively, whereas a lower proportion of cells in G2 phase (31.25%) in comparison to the control (24.87% in G1, 15.27% in S, and 34.44% in G2). According to DFT analysis, the synthesized compounds have been found to show activity comparable to the standard drug, erlotinib. Likewise, the compounds interact well with the target protein (EGFR) through key amino acid residues with binding energies between –10.2 and –7.3 Kcal/mol and show the appropriate ADMET properties.

Keywords: Acetylcoumarin, Anticancer, Hydroxycoumarin, Molecular Docking, Schiff base

Cancer is an unchecked, accelerated, and abnormal cell proliferation that often invades and kills healthy body cells. It is the main cause of death in the general population worldwide in both developed and developing nations. There has been significant advancement in the detection, prevention, and treatment of cancer, as well as the identification of medicines for the disease, unfortunately, there are still many kinds of cancer that cannot be cured[1]. Transduction of cell signals is a basic mechanism in the initiation and spread of cancer[2]. Cancer possesses a relentless ability to invade and spread throughout the body, making it one of the foremost causes of mortality worldwide. According to the World Health Organization, this formidable disease is recognized as one of the greatest health challenges, affecting one in eight men and one in eleven women. These staggering statistics highlight the urgent need for awareness, research, and innovative treatments to combat this pervasive illness that touches so many lives[3]. The compounds based on hydroxycoumarin have the potential to exhibit significant cytotoxic effects on several cancer cell lines, including Hela, MCF-7, promyelocytelukemia-derived (HL-60), urinary bladder carcinoma-derived (EJ)[4]. Chemoprevention is a strategy that uses natural, synthetic, or biological agents to stop or slow down the development of cancer. This approach has led to a growing interest in understanding how cancer forms, helping researchers identify targets to interrupt this process[5]. Even though chemotherapy has drawbacks such as drug resistance and drug-induced toxicity, it is currently the most important method for treating cancer[6]. Anticancer drugs are typically made to interfere with the process of cell division in order to target and kill the cells that divide abnormally. Some of these drugs, such as coumarins function as cross-linking or DNA intercalating agents and form intra-strand and inter-strand connections[7].

Coumarins are secondary metabolites found in a wide variety of plant species, and are most prevalent in the Apiaceae, Rutaceae, Asteraceae, and Fabaceae

families[8]. In medicinal chemistry, Schiff bases are an important class of chemicals. It is predictable that coumarins with a Schiff base moiety exhibit enhanced anticancer and other unique properties[9]. The capacity of Schiff bases to stabilize nearly multiple metal ions in a variety of oxidation states, their high solubility in common solvents, and their varied production make them "privileged ligands". Using Schiff bases, several possible medications are obtained[10]. The coumarins' broad spectrum of biological activities and applications can be attributed to their capacity to form noncovalent interactions with several enzymes and receptors in living beings. The current developments of coumarin derivatives include a wide range of medicinal chemistry, including anticancer, antioxidant, anticoagulant, antiviral, anti-inflammatory, anti-neurodegerative, anti-diabetics, antifungal and antibacterial, agents[11]. Coumarin compounds can stop the growth, proliferation, and metastasis of different tumor cells through a variety of mechanisms, including inhibition of the PI3K/ AKT/ mTOR signaling pathway, microtubule polymerization, angiogenesis, aromatase inhibition, acting on apoptosis proteins, multidrug resistance, and others[12].

The ligands and their copper complexes synthesized from 3-acetylcoumarin and different thiosemicarbazides, exhibited strong anticancer efficacy with IC_{50} value 32.84 - 42.71 µg/mL when tested against MCF-7 cell lines[13]. The thiosemicarbazones and Schiff bases obtained from 3-acetylcoumarin showed drug-like activity based on ADMET prediction and their low band gap energy of HOMO and LUMO (4.26 eV-2.64 eV), support their effective reactivity[14.] Hydroxyurea, is an anticancer medicinal molecule used to treat cervical cancer, sickle-cell disease, and chronic myelogenous leukemia[15]. The novel 4-hydroxycoumarin derivatives, along with their ligands and copper complexes, were subjected to Western blot analysis. The results indicated that these compounds play a crucial role in the progression of cell apoptosis[16]. Urea has become a key scaffold in medicinal chemistry, because of its unique drug-target interactions, favorable physicochemical properties that enhance the drug ability of new compounds, and structural versatility that opens up numerous drug design opportunities[17]. Thiourea is an important molecule that is utilized as a fundamental building block to prepare a variety of derivatives with various biological activity, these derivatives have been shown to have strong anticancer and antibacterial properties[18].

This paper describes the synthesis, structure elucidation and anticancer screening of Schiff bases of urea, thiourea and hydroxyurea with 4-hydroxycoumarin and 7-hydroxycoumarin moieties. The anticancer activities of the compounds against breast cancer cell line, DFT calculations and pharmacokinetics are reported.

Experimental Section

All chemicals utilized were of analytical reagent grade (AR). 4-Hydroxycoumarin (98%) and 7-hydroxycoumarin (98%) were procured from Alfa Aesar, while ethyl alcohol (99%) was sourced from Merck, pyridine, hydrochloric acid from Qualigens, and glacial acetic acid (99.7%), acetyl chloride (99%), from Fischer Scientific, and urea, thiourea, hydroxyurea (Alfa Aesar) were used as received. MTT (>97%) and DMSO (99.9%) were obtained from Genetics Biotech Pvt. Ltd. DMEM, NEAA, and FBS were sourced from Gibco, and Penicillin-streptomycin from Sigma. MCF-7 cell lines were acquired from Aakaar Biotechnologies Pvt. Ltd., Lucknow, Uttar Pradesh, India. CHNS analysis by Elementar Vario EL III CHNS analyzer (IIT Madras, India). The FTIR spectra were obtained using the Shimadzu IR Tracer-100 instrument (resolution 0.25 cm^{-1}, SN ratio 60,000:1) covering the wave number range of 4000-400 cm^{-1} at the Nepal Academy of Science and Technology (NAST), Kathmandu, Nepal. The absorption bands in the UV-Vis spectra of compounds were measured using the Agilent Technologies Carry 60 UV-Vis spectrometer (1.5 nm fixed spectral bandwidth, wavelength range 190-1100 nm) at the Central Department of Chemistry, Tribhuvan University (T.U.), Kathmandu, Nepal. Data analysis for UV-Vis and FT-IR spectra was conducted using Origin Pro software, while IC_{50} values were determined using Graph Pad Prism software. Melting points were determined using a Philips Harris melting point apparatus. NMR spectra were recorded using a Bruker Bio Spin GmbH NMR spectrometer (400 MHz) at the NMR Research Center, Indian Institute of Science, Bangalore, India. Elemental analysis (CHNS) by Elementar Vario EL III CHNS analyzer, and ESI-HRMS analysis was performed using an LC-QTOF-HRMS spectrometer (TOF Mass range *m/z* 20 to 1,00,000; Quadrupole mass range *m/z* 20-16,000; Resolving power >40,000 FWHM; Mass accuracy >1ppm), Indian Institute of Technology, Madras, India.

Acetylation of hydroxycoumarin

A solution comprising 4-hydroxycoumarin/ 7-hydroxycoumarin (0.064 mol. 10.4 g) dissolved in a solvent, dry pyridine (80 mL) and the catalyst piperidine (0.01 mL), was cooled to 0-5°C. Then, acetyl chloride (0.094 mol. 7.4 g) was added, and the mixture was stirred for 48 hours at RT. The resultant dark red/brown reaction mixture was poured onto ice/water (234 mL), and the product was adjusted to *p*H 1-2 using 2 N hydrochloric acid. The resulting precipitate was filtered under suction, washed with water until neutral, and then dried. The yield was 62%, and recrystallization in ethanol/water (1:1), produced crystals with a recorded melting point of 136-138°C (lit. m. p. 134-136°C)[19] (Scheme 1).

Synthesis of compounds SB1, SB2, SB3, SB4

Urea 5 mmol (0.30 g)/ thiourea (0.38 g) was dissolved in 10 mL ethanol, 10 mmol of 3-acetyl-4-hydroxycoumarin (2.04 g)/10 mmol of 3-acetyl-7-hydroxycoumarin (obtained by Scheme 1) (2.04 g) was dissolved in 10 mL ethanol. These two solutions were mixed in a round-bottomed flask and refluxed for 2 h. Then the mixture was allowed to cool at RT and the precipitate was filtered off, washed with cold ethanol and dried in a desiccator overnight[20] (Scheme 2).

Synthesis of compounds SB5, SB6, SB7

3-Acetyl-4-hydroxycoumarin/ 3-acetyl-7-hydroxycoumarin (2.5 mmol, 0.51 g) was added to the solution of hydroxyurea (2.5 mmol, 0.19 g) in 15 mL absolute ethanol. The mixture with catalytic amount (0.1 mL) of acetic acid, was continuously stirred on hot plate and then refluxed for 5 h at 78-80°C. The precipitate was filtered, dried at 40°C overnight and recrystallized from ethanol[21,22] (Scheme 3).

Pharmacokinetics Studies

For the chemical library of the synthesized compounds including reference drug, SMILES (Simplified Molecular Line Entry System) were automatically generated from their Chemdraw structures and their pharmacokinetics (ADMET) profile were studied employing accessible tool, pkCSM https://biosig.lab.uq.edu.au/pkcsm/prediction. For ADMET profile, parameters like water solubility, Caco-2 permeability, intestinal absorption, volume of distribution (VDss), blood brain barrier (BBB) permeability, central nervous system (CNS) permeability, cytochrome P450, total clearance, Ames toxicity and hepatotoxicity were analyzed.

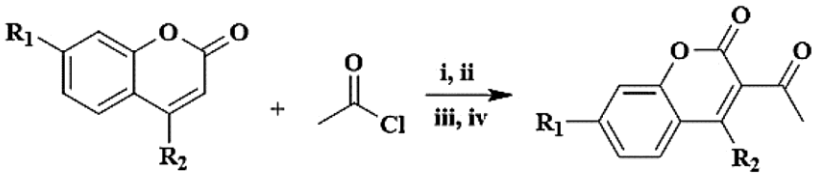

R_1 / R_2 = H/OH, (i) pyridine, (ii) piperidine, (iii) stir, 48 h, (iv) room temperature

Scheme 1 — Acetylation of hydroxycoumarin

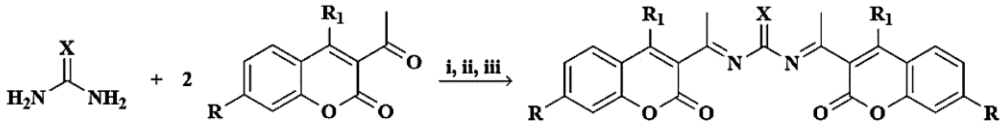

R and R_1 = H and OH (SB1and SB2); R and R_1 = OH and H (SB3 and SB4); X = O (SB1, SB3), S (SB2, SB4); (i) Ethanol, (ii) AcOH, (iii) Reflux, 2 h

Scheme 2 — Synthesis of Schiff bases from urea and thiourea

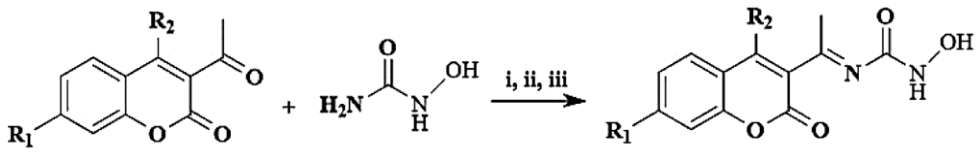

R_1 and R_2 = H and OH (SB5); R_1 and R_2 = OH and H (SB6); R_1 = R_2 = H (SB7); (i) Ethanol, (ii) AcOH, (iii) Reflux, 5 h

Scheme 3 — Synthesis of Schiff bases from hydroxyurea

Molecular Docking

The 3D structures of the synthesized compounds were generated Chem3D Pro 12.0 which were saved in .pdb format and optimized in AutoDockTools 1.5.7[23], then saved in .pdbqt format. The therapeutic target, 4HJO (Crystal structure of the inactive EGFR tyrosine kinase domain with erlotinib) of resolution 2.75 Å was attained from the RCSB PDB database. The EGFR were prepared in BIOVIA Discovery Studio where all the chains, water molecules and crystalline structures other than target protein were detached from the retrieved structure and saved in .pdb format. The system becomes simpler when water molecules are eliminated, which improve the efficiency and lowers the computational burden of the docking process. The structures were saved in .pdbqt format after optimizing with Kollmann charges and adding polar hydrogen in AutoDock Tools 1.5.7 (https://vina.scripps.edu/). Adding polar hydrogen on amino acid residues can have a substantial impact on the activity and binding affinity of protein and ligand. A grid box containing the important amino acid residues of target protein was established, with a spacing of 0.375 Å and a dimension of 40 × 40 × 40 Å, and the compounds were docked around the targeted binding pocket of protein. The binding site that was selected was the binding pocket of the co-crystallized ligand and the grid box covered all the binding sites. To reduce the possibility of undesirable docking outcomes, the re-docking technique was first used to validate the docking approach and superimposition techniques (RMSD ≤ 2 Å) of co-crystallized ligands in 4HJO, which validated the docking protocol[24]. The structures and orientation of the compounds within protein sites were thoroughly investigated prior to binding affinity study.

Density Functional Theory (DFT) Calculations

With the aid of GaussView 6.0 and Gaussian 09 program, the three dimensional structures of the synthesized compounds were optimized http://www.gaussian.com/. For the optimization and frequency calculations, the 6-31G' (d, p) basic set and B3LYP method which is an acronym for Becke's three-parameter were selected. The B3LYP functional technique offers an accurate and efficient computation[25]. Using the same level of theory, the frontier molecular orbitals, HOMO and LUMO orbitals, of the synthesized compounds were determined and band gap (ΔE) and HOMO-LUMO energy levels were used to assess chemical reactivity. Additionally, using the DFT method, the molecular electrostatic potential (MEP) map was examined in order to identify the reactive zones of compounds for electrophilic and nucleophilic attack reaction regions. The optimized geometry, HOMO-LUMO, and MEP were visualized using the GaussView 6.0 graphical interface.

Results and Discussion

1,3-bis[(1*E*)-1-(4-Hydroxy-2-oxo-2*H*-chromen-3-yl) ethylidene]urea, SB1, (Fig. 1)

It was prepared as shown in Scheme 2, by refluxing a mixture of urea and 3-acetyl-4-hydroxycoumarin

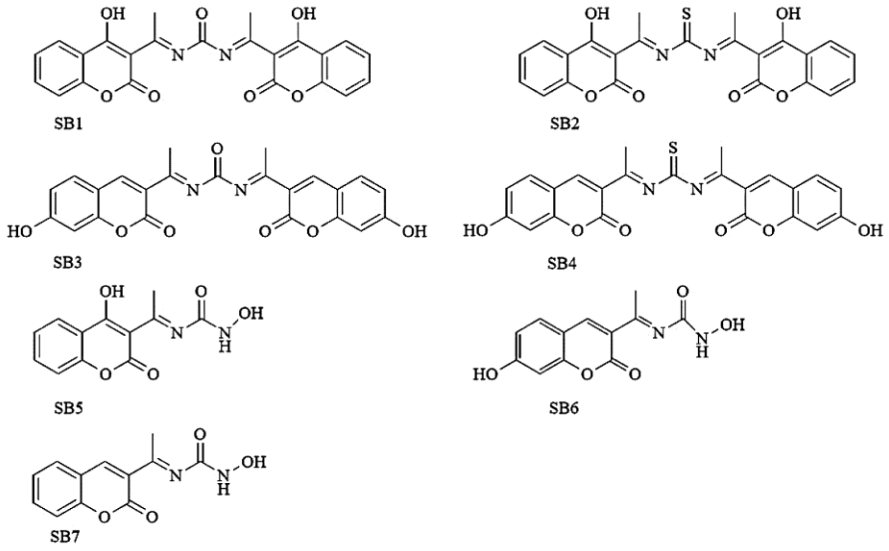

Fig. 1 — Structure of the synthesized Schiff bases

(1:2) in ethanol. The separated solid was filtered, dried, and recrystallized from ethanol. Yield 82%. m.p. 184°C. State: powder. Elemental analysis: [$C_{23}H_{16}N_2O_7$] % found (calculated): C, 63.85 (63.89); H, 3.70 (3.73); N, 6.41 (6.48). ESI-HRMS: positive mode, found (calculated) *m/z* 433.1017 (433.1030) $[M+H]^+$; ^{1}H NMR (400 MHz, DMSO-d_6): δ 13.62 (s, 2H, OH), 7.99, 7.85, 7.45, 7.41(m, 8H Ar-H), 2.66 (s, 6H, CH_3-C=N, C12-H, C12′-H); ^{13}C NMR (400 MHz, DMSO-d_6): δ 162.53 (C=O, urea moiety), 159.18 (C=O, lactone), 154.17 (C=N), 147.08 (pyran, C3), 136.69 (C4), 125.21 (C10), 124.78 (C7), 116.85 (C6), 114.77 (C5), 110.56 (C8), 101.45 (C9) (Ar-C), 29.62 (CH_3- C12, C12′); IR: 3401 (b, O-H), 3077 (CH, Ar), 1729 (C=O, lactone), 1670 (s, CO, urea moiety), 1602 (s, C=N), 1109, 1024 cm^{-1} (s, C-O, ester); UV-Vis (methanol, λmax nm): 300s (π-π*), 321sh (n- π*).

1,3-bis[(1*E*)-1-(4-Hydroxy-2-oxo-2*H*-chromen-3-yl)ethylidene]thiourea, SB2, (Fig. 1)

It was prepared as shown in Scheme 2, by refluxing a mixture of thiourea and 3-acetyl-4-hydroxycoumarin (1:2) in ethanol. The separated solid was filtered, dried, and recrystallized from ethanol. Yield 79%. m.p. 188°C. State: powder. Elemental analysis: [$C_{23}H_{16}N_2O_6S$] % found (calculated); C, 61.64 (61.60); H, 3.63 (3.60); N, 6.21 (6.25); S, 7.12 (7.15). ESI-HRMS: positive mode, found (calculated) *m/z* 449.0822 (449.0801) $[M+H]^+$; ^{1}H NMR (400 MHz, DMSO-d_6): δ 13.49 (s, 2H, OH), 8.00, 7.83, 7.46, 7.42 (m, 8H Ar-H), 2.67 (s, 6H, CH_3-C=N, C12-H, C12′-H); ^{13}C NMR (400 MHz, DMSO-d_6): δ 178.33 (C=S), 159.74 (C=O, lactone), 154.09 (C=N), 147.10 (pyran, C3), 136.58 (C4), 125.35 (C10), 124.29 (C7), 117.29 (C6), 114.06 (C5), 110.93 (C8), 110.20 (C9) (Ar-C), 29.48 (CH_3- C12, C12′); IR: 3400 (b, O-H), 3082 (CH, Ar), 1741 (C=O, lactone), 1618 (s, C=N), 1267 (C=S, thiourea moiety), 1200, 1119 cm^{-1} (s, C-O, ester); UV-Vis (methanol, λmax nm): 300s (π-π*), 325sh (n- π*).

1,3-bis[(1*E*)-1-(7-Hydroxy-2-oxo-2*H*-chromen-3-yl) ethylidene]urea, SB3, (Fig. 1)

It was prepared as shown in Scheme 2, by refluxing a mixture of urea and 3-acetyl-4-hydroxycoumarin (1:2) in ethanol, Yield 83%. m.p. 186°C. State: powder. Elemental analysis: [$C_{23}H_{16}N_2O_7$] % found (calculated); C, 63.86 (63.89); H, 3.76 (3.73); N, 6.45 (6.48). ESI-HRMS: positive mode, found (calculated) *m/z* 433.1006 (433.1030) $[M+H]^+$; ^{1}H NMR (400 MHz, DMSO-d_6): δ 10.57 (s, 2H, OH), 7.94 (2H, C4-H, C4′-H), 7.28, 7.15, 6.79 (m, 6H Ar-H), 2.30 (s, 6H, CH_3-C=N, C12-H, C12′-H); ^{13}C NMR (400 MHz, DMSO-d_6): δ 168.82 (C=O, urea moiety), 159.72 (C=O, lactone), 154.07 (C=N), 152.88 (pyran, C3), 143.84 (C4), 129.72 (C7), 118.69 (C10), 116.66 (C5), 113.11 (C6), 111.40 (C9), 110.14 (C8), (Ar-C), 20.87 (CH3-C12, C12′); IR: 3265 (b, O-H), 3054 (CH,Ar), 1725 (C=O, lactone), 1607 (s, C=N), 1106, 1035 cm^{-1} (s, C-O-C, ester); UV-Vis (methanol, λmax nm): 282br (π-π*), 313br (n- π*).

1,3-bis[(1*E*)-1-(7-Hydroxy-2-oxo-2*H*-chromen-3-yl) ethylidene]thiourea, SB4, (Fig. 1)

It was prepared as shown in Scheme 2, by refluxing a mixture of thiourea and 3-acetyl-4-hydroxycoumarin (1:2) in ethanol. Yield 78%. m.p. 187°C. State: powder. Elemental analysis: [$C_{23}H_{16}N_2O_6S$] % found (calculated); C, 61.63 (61.60); H, 3.64 (3.60); N, 6.23 (6.25); S, 7.12 (7.15). ESI-HRMS: positive mode, found (calculated) *m/z* 449.0827 (449.0801) $[M+H]^+$; ^{1}H NMR (400 MHz, DMSO-d_6): δ 10.57 (s, 2H, OH), 8.05 (2H, C4-H, C4′-H), 7.26, 7.17, 6.48 (m, 6H Ar-H), 2.30 (s, 6H, CH_3-C=N, C12-H, C12′-H); ^{13}C NMR (400 MHz, DMSO-d_6): δ 179.37, (C=S), 159.65 (C=O, lactone), 154.03 (C=N), 152.84 (pyran, C3), 143.76 (C4), 129.27 (C7), 118.60 (C10), 116.60 (C5), 115.49 (C6), 110.06 (C9), 102.08 (C8) (Ar-C), 20.81 (CH_3- C12, C12′); IR: 3265 (b, O-H), 3054 (CH, Ar), 1718 (C=O, lactone), 1605 (s, C=N), 1254 (C=S, thiourea moiety), 1105, 1034 cm^{-1} (s, C-O-C, ester); UV-Vis (methanol, λmax nm): 282br (π-π*), 312br (n- π*).

1-Hydroxy-3-[(1*E*)-1-(4-hydroxy-2-oxo-2*H*-chromen-3-yl)ethylidene]urea, SB5, (Fig. 1)

It was prepared as shown in Scheme 3, by refluxing a mixture of hydroxyurea and 3-acetyl-4-hydroxycoumarin (1:1) in ethanol. Yield 74%. m.p. 190°C. State: powder. Elemental analysis: [$C_{12}H_{10}N_2O_5$] % found (calculated); C, 54.94 (54.97); H, 3.86 (3.84); N, 10.65 (10.68). ESI-HRMS: positive mode, found (calculated) *m/z* 263.0679 (263.0662) $[M+H]^+$; ^{1}H NMR (400 MHz, DMSO-d_6): δ 13.51 (s, H, OH), 10.54 (NH/OH), 7.99, 7.85, 7.82, 7.43 (m, 4H Ar-H), 2.67 (s, 3H, CH_3-C=N, C12-H); ^{13}C NMR (400 MHz, DMSO-d_6): δ 162.10 (C=O, urea moiety), 159.11 (C=O, lactone), 154.12 (C=N), 146.59 (pyran, C3), 136.63 (C4), 133.12 (C10), 125.14 (C7), 124.72 (C6), 116.79 (C5), 114.69 (C8), 110.42 (C9), (Ar-C), 29.52 (CH_3-C12); IR: 3428 (b, O-H), 3326 (N-H, N2), 1731 (C=O, lactone), 1605 (s, C=N), 1251 (OH),

1105, 1031 cm^{-1} (s, C-O-C, ester); UV-Vis (methanol, λmax nm): 300s (π-π*), 324sh (n- π*).

1-Hydroxy-3-[(1*E*)-1-(7-hydroxy-2-oxo-2*H*-chromen-3-yl)ethylidene]urea, SB6, (Fig. 1)

It was prepared as shown in Scheme 3, by refluxing a mixture of hydroxyurea and 3-acetyl-4-hydroxycoumarin (1:1) in ethanol. Yield 75%. m.p. 191°C. State: powder. Elemental analysis: [$C_{12}H_{10}N_2O_5$] % found (calculated); C, 54.95 (54.97); H, 3.86 (3.84); N, 10.64 (10.68). ESI-HRMS: positive mode, found (calculated) *m/z* 263.0693 (263.0662) $[M+H]^+$; ^{1}H NMR (400 MHz, DMSO-d_6): δ 10.48 (s, H, OH), 8.23 (1H, NH), 7.94 (1H, C4-H), 7.53, 6.88, 6.77 (m, 3H, Ar-H), 1.90 (s, 3H, CH_3-C=N, C12-H); ^{13}C NMR (400 MHz, DMSO-d_6): δ 161.32 (C=O, urea moiety), 160.44 (C=O, lactone), 155.50 (C=N), 144.55 (pyran, C3), 136.60 (C4), 129.72 (C7), 125.36 (10), 116.22 (C5), 113.13 (C6), 111.39 (C9), 102.15 (C8), (Ar-C), 29.49 (CH_3-C12); IR: 3161 (b, OH/NH), 3082 (CH, Ar), 1678 (C=O, lactone), 1624 (s, C=N), 1240 (OH), 1203, 1113 cm^{-1} (s, C-O, ester); UV-Vis (methanol, λmax nm): 281br (π-π*), 313br (n- π*).

1-Hydroxy-3-[(1*E*)-1-(2-oxo-2*H*-chromen-3-yl) ethylidene]urea, SB7, (Fig. 1)

The Schiff base, SB7 was prepared by refluxing the solution of 3-acetylcoumarin and hydroxyurea (1:1, molar ratio) in ethanol at 80°C for 2 h, Scheme 3. Yield 65%. m.p. 172°C. State: powder. Elemental analysis: [$C_{12}H_{10}N_2O_4$] % found (calculated); C, 58.57 (58.54); H, 4.05(4.09); N, 11.34 (11.38). ESI-HRMS: positive mode, found (calculated) *m/z* 247.0819 (247.0713) $[M+H]^+$; ^{1}H NMR (400 MHz, DMSO-d_6): δ 10.51 (s, H, OH), 8.65 (1H, NH), 7.95 (1H, C4-H), 7.75, 7.73, 7.46, 7.41 (m, 4H Ar-H), 2.58 (s, 3H, CH_3-C=N, C12-H); ^{13}C NMR (400 MHz, DMSO-d_6): δ 162.54 (C=O, urea moiety), 158.43 (C=O, lactone), 154.59 (C=N), 147.05 (pyran, C3), 136.22 (C4), 134.48 (C10), 130.77 (C7), 124.93 (C5), 118.15 (C6), 116.10 (C9), 110.22 (C8), (Ar-C), 30.05 (CH_3-C12); IR: 3441 (b, O-H), 3378 (N-H, N2), 1736 (C=O, lactone), 1618 (s, C=N), 1269 (OH), 1199, 1116 cm^{-1} (s, C-O, ester); UV-Vis (methanol, λmax nm): 298br (π-π*), 340sh (n- π*).

ESI-HRMS

High resolution mass spectrometry (HRMS) using electrospray ionization (ESI) in positive mode and Quadrupole Time-of-Flight (QTOF) was employed to confirm the molecular masses of the synthesized Schiff bases. This technique provides specificity, high sensitivity, and accurate mass determination[26]. The soft ionization conditions produced protonated molecular ions with minimal fragmentation, resulting in a single, well-defined peak for each compound. The protonated molecular ion $[M+H]^+$ peaks for the new compounds SB1, SB2, SB3, SB4, SB5, SB6, SB7; *m/z*: calculated (found); 433.1030 (433.1017), 449.0801 (449.0822), 433.1030 (433.1006), 449.0801 (449.0827), 263.0662 (263.0679), 263.0662 (263.0693), 247.0713 (247.0819), respectively were obtained[27]. These values closely matched the theoretical masses, confirming the successful synthesis of the target compounds (**Supplementary Information S1-S7**).

NMR spectroscopy

The ^{1}H NMR spectrum of the synthesized compounds was recorded in DMSO. Methyl protons were assigned as a singlet at δ 2.30 for the compounds SB3 and SB4[28], δ 2.67-2.58 for SB1, SB2, SB5, SB7 and δ 1.90 for the compound SB6[29]. Protons linked to carbons that are adjacent to sp^2 or sp hybridized carbons or the part of a conjugated system can also resonate at higher δ values due to the increased deshielding effects. The methyl group is directly linked to the imine group (C=N), which originates a deshielding effect due to the electron-withdrawing nature. The singlet or doublet signals in the range of δ 8.05-6.48 reveals the aromatic protons[30]. This chemical shift is characteristic of protons attached to a benzene ring, influenced by the resonance effect and electron-withdrawing effects of adjacent functional groups. In proton NMR spectra of SB5, and SB6, the NH and OH groups exhibited chemical shifts of δ 10.54, and δ 10.48, respectively, reflecting their similar hydrogen bonding environments and the influence of electronegativity on their respective proton resonances[16]. The spectra of SB7, exhibited a broad singlet at δ 8.65 corresponding to NH proton[15]. The ^{1}H NMR spectrum of SB1, SB2 and SB5 displayed signals due to phenolic OH proton downfield singlet at δ 13.62-13.49 (Ref. 10), whereas for the compounds SB3, SB4, and SB6, phenolic OH proton signals were observed as singlet at δ 10.57-10.48 (Ref. 31). In 4-hydroxycoumarin, the hydroxyl group is positioned perpendicular to the carbonyl group. This close proximity allows for strong intramolecular hydrogen bonds, that stabilizes the hydroxyl group and shift its resonance downfield, whereas 7-hydroxycoumarin has a more protected

environment and weaker interactions because the hydroxyl group is farther from the carbonyl group (**Supplementary Information S8-S14**).

The number of magnetically non-equivalent carbon atoms in the synthesized compounds is shown by the number of peaks in the ^{13}C NMR spectra. In the ^{13}C NMR spectra, (C12, C12′) CH_3 of SB1, SB2, SB5, SB6, and SB7 were exhibited at δ 30.05-29.48 (Ref. 32), it is possibly due to the electronegative nitrogen atom linked to the adjacent carbon. The methyl carbons peaks for SB3 and SB4, were noticed at δ 20.87 and 20.81, respectively. The spectra of the compounds SB1-SB7, exhibited resonance due to highly polar carbonyl (C=O, lactone), carbons towards downfield region at δ 160.44-158.43, and due to thiocarbonyl (C=S), of SB2 and SB4 at δ 178.33 and 179.37, respectively[33]. The chemical shift of the carbonyl carbon (C=O) of acetyl group, was detected at δ 195.38 downfield[32]. The disappearance of this band and appearance of new peaks at δ 155.50-154.03 which is attributed to imine group (C=N), confirmed the formation of Schiff bases. The chemical shifts of the carbonyl (urea moiety) of the compounds SB1, SB3, SB5, SB6, and SB7, were appeared at δ 168.82-161.32 (Ref. 34). The carbon peaks on the benzene rings were found at δ 136.60-101.45, which was in accordance with the aromatic carbon atom peaks that have been documented[35]. The chemical shifts of pyran carbons, appeared at δ 152.88-144.55 (C3) and 143.84-136.22 (C4)[36]. These specific shifts indicate that the carbons are probably involved in the conjugated π-system and are influenced by nearby functional groups. The E form is the more stable diastereoisomer in the majority of Schiff bases because the Z diastereoisomer of a hydrazone bond is a momentary species[37] (**Supplementary Information S15-S21**).

FT-IR spectroscopy

FT-IR spectra of the compounds SB1, SB2, SB5, SB7 showed broad bands at 3401, 3400, 3428, and 3441 cm^{-1}, respectively which were assigned to υ(OH) of phenolic groups[38]. Due to the different binding strengths, the O-H bond being stronger, its stretching vibration in the FTIR spectra was at a higher wavenumber than the υ(NH) stretching vibration[39], whereas for the compounds SB3, SB4, SB6, these bands were observed at 3265-3161 cm^{-1} [40]. It was observed that the band corresponding to υ(OH) was attenuated and shifted towards a lower wave number. Normally, this band would be at around 3600 cm^{-1} in the absence of intramolecular or intermolecular hydrogen bonding[41]. The molecule 3-acetylcoumarin's infrared spectra showed a significant band at 1686 cm^{-1}, which corresponded to the acetyl group's υ(C=O) stretching[32]. When it was condensed with urea, thiourea and hydroxyurea a new stretching frequency appeared at 1624-1602 cm^{-1}, which suggested the formation of an imine bond (C=N)[41]. The emergence of these bands and the elimination of the predicted bands, -NH2 and -CH3C=O, in the spectra, confirmed the formation of the target compounds[42]. The band observed at 1251, 1240, and 1269 cm^{-1}, for the compounds SB5, SB6 and SB7 respectively, assigned to the stretching frequency of phenolic C-OH bond[43]. The aromatic υ(C-H) stretching at 3082-3054 cm^{-1} and pyran C-O stretching at 1203-1024 cm^{-1} were noted[44]. The stretching frequencies of υ(C=O, lactone) for the synthesized compounds were shown at 1741-1678 cm^{-1}, and the sharp band appeared at 1670 cm^{-1}, is attributed to υ(C=O, urea moiety) of the compound, (SB1)[45,46]. The NH group of compounds SB5 and SB7 displayed absorptions at 3326 and 3378 cm^{-1}, respectively[47]. The bands observed at 1267 and 1254 cm^{-1}, were assigned to υ(C=S), thiourea moiety, for the compounds SB2 and SB4 respectively[28]. The FTIR value for the υ(C=S) stretching vibration of the thiourea moiety is in agreement with values found in the literature and is consistent with the expected behavior of the C=S bond in thiourea-based compounds. The υ(C=S) stretching vibration appears in the range of 1200-1350 cm^{-1}, depending on the electronic environment surrounding the thiourea group (**Supplementary Information S22-S28**).

UV-Vis spectroscopy

The UV-Vis spectra of the synthesized Schiff bases (SB1- SB7) showed absorption peaks at 281-300 and 312-340 nm in methanol. The absorption band at 281-300 nm is attributed to $\pi \rightarrow \pi^*$ transition within coumarin moiety. The absorption band appeared at 312-340 nm, was assigned to $n \rightarrow \pi^*$ transitions of C=O (urea moiety), C=O (coumarin), C=N (azomethine) or C=S (thiourea moiety)[20,41,48]. It is influenced by the extended conjugation between coumarin ring and amine. In thiourea derivative a bathochromic shift was observed that shifts the transitions to slightly longer wavelengths because of conjugation from thiourea moiety and the high polarizability of sulphur. In hydroxyl urea derivative (SB5), the OH group may be involved in hydrogen

bonding that alters the conjugation and electron density, resulting in a slight bathochromic shift. The C=O group shows n → π* electronic transition at a lower wavelength, whereas the C=S moiety, associated with lower energy of lone pair electrons at sulphur, shows this transition at a longer wavelength. The intramolecular charge transfer (ICT) causes movement of electron density from electron-donor groups like OH, NH_2 to electron-acceptor groups like C=N, C=O within the molecule. The longer wavelength band at 324-340 nm is due to an intramolecular charge transfer within the molecule[49]. This ICT phenomenon is also responsible for the broadening of absorption peaks. The broadening of absorption peaks is also due to the solute-solvent interaction. As well as the broadening of the peak is due to the overlapping transition of n → π* of C=N (imine) and charge transfer from electron donor OH, C=O to electron acceptor C=N. Methanol, being polar protic solvent, causes dipole-dipole interactions and can form hydrogen bond, stabilizes excited state. This stabilization decreases the energy required to promote the molecule to the excited state, and it results in a bathochromic shift[50] (**Supplementary Information S29-S35**).

In vitro cytotoxicity assay (MTT assay)

The MTT assay was used to assess the cytotoxicity of the newly synthesized coumarin derivatives on the MCF-7 cell line (purchased from NCCS Pune) (Fig. 2). The cells (1×10^4 cells per well) were grown in Dulbecco's modified Eagle's medium (DMEM) supplemented with 10% fetal bovine serum (FBS) and 1% antibiotic solution (penicillin- streptomycin) at 37°C with 5% CO_2 for 24 hours in a 96-well plate with four replicates. The following day, various concentrations of the compounds prepared in an incomplete medium were applied to the cells. Treatment-free cells were referred to as Control cells, and MTT-free cells were referred to as Blank cells.

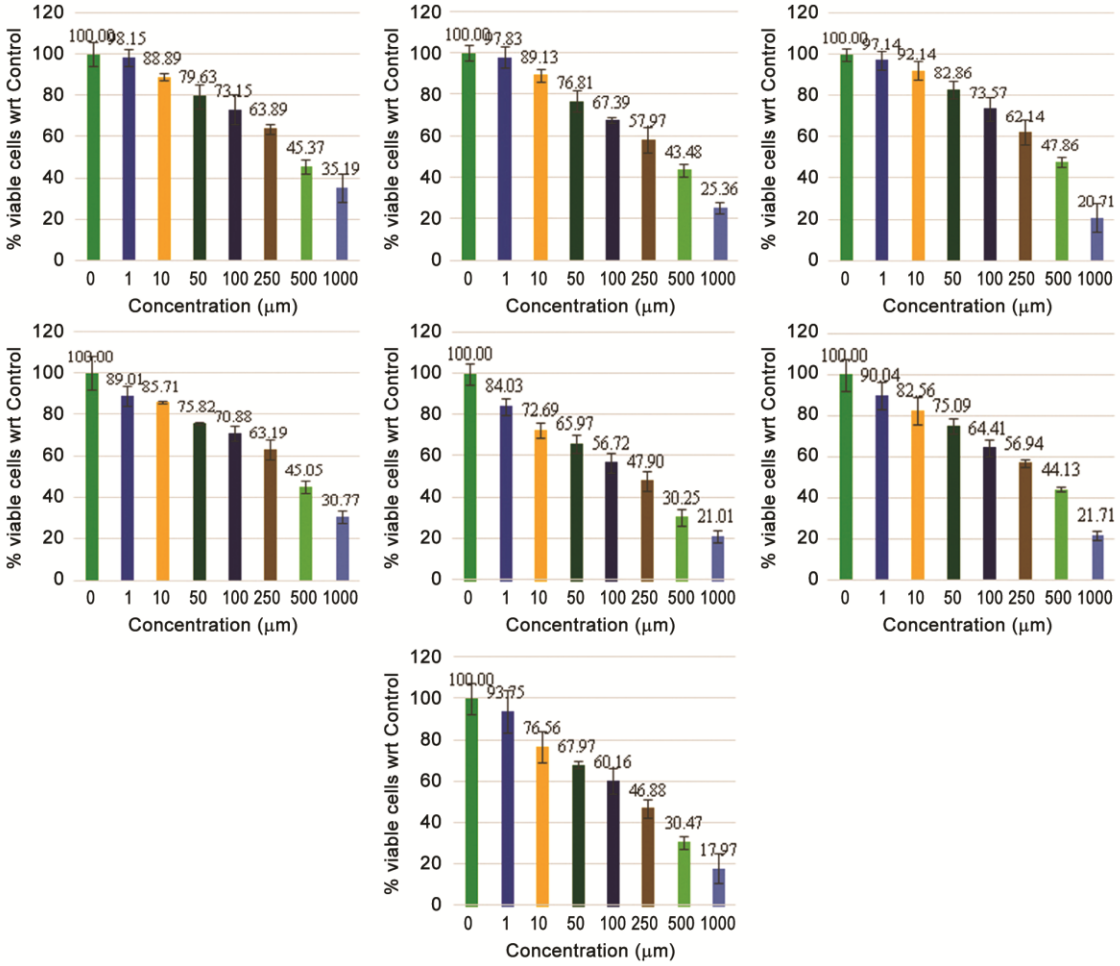

Fig. 2 — Cell viability assay (MCF-7) of synthesized compounds (SB1-SB7) at different concentrations

Following a 24-hour incubation period, the cell culture was treated with MTT 3-(4,5-dimethylthiazol-2-yl)-2,5-diphenyl-2*H*-tetrazolium bromide) solution at a final concentration of 250 µg/mL, and the mixture was incubated for an additional 2 hours. Four replicates were carried out for each compound against the cell line. The culture supernatant was discarded at the end of the experiment, and the cell layer matrix was dissolved in 100 µL of dimethyl sulfoxide (DMSO, Merck)) and measured at 540 nm using an Elisa plate reader (iMark, Biorad, USA). With the use of GraphPad Prism 6, the IC_{50} was computed. Using a camera (AmScope digital camera 10 MP Aptima CMOS), images were taken under an inverted microscope (Olympus eK2). The anticancer activity of each compound was calculated as the mean of four replicates. The 50% inhibitory concentration (IC_{50}) was expressed as the mean ± Standard Error of Mean of the data[51,52]. Percentage viability of the cells was calculated using the formula, % viable cells = $(OD_{sample}/OD_{control}) \times 100$).

Cell cycle analysis

The most active compound (SB5) was subjected to cell cycle analysis to know the mechanisms of action at different phases of the cell cycle. Cells were plated and treated with the compound, SB5 for 24 hours. Cells without treatment were considered as Control. After incubation period, cells were harvested using the trypsin and collected in 1.5 mL tube and washed once with 500 µL chilled PBS. Approximately, 10^6 cells were suspended in 100 µL of PBS, and vortexed gently to obtain a mono-dispersed cell suspension, with minimal cell aggregation. Cells were then fixed by transferring this suspension, with a pipette, into centrifuge tubes containing 900 µL of 70% ethanol, on ice and incubated for at least 2 h at 4°C. Cells can be stored in 70% ethanol at 4°C for several weeks. After fixation, cell was centrifuged and pellet was suspended in 500 µL of Propidium Iodide (PI) staining solution 0.1% (v/v) Triton X-100, 10 µg/mL PI and 100 µg/mL DNase-free RNaseA in PBS) and kept in the dark at RT for 30 min, or at 37°C for 10 min. The compound, SB5 then acquired on a flow cytometer (BD FACSCalibur)[53]. A gating approach was implemented to eliminate doublets and debris, ensuring that only single, live cells were included in the analysis. 10,000 events were collected per sample to determine the proportion of cells in G0/G1, S, and G2/M phases.

G1/S and G2/M are two crucial regulatory phases of the normal cell cycle, which is made up of G1-S-G2-M. When this regulatory function is lost, tumours can develop[54]. The unchecked cell proliferation cycle is linked to the endless proliferation features of malignant tumours under *in vitro* growth conditions. The secret to preventing tumour cell development and proliferation is to restrict the progression of the cell cycle[55]. The majority of chemotherapy medications have antitumor properties and can induce cell cycle arrest.

After the SB5 treatment, the cell cycle distribution in several phases was examined to gain a better understanding of the mechanism underlying the reduction in cell proliferation. When compared to untreated cells, MCF-7 cells treated with SB5 exhibited significant alterations in their cell cycle, including a rise in the proportion of cells in the G2/M phase and a corresponding decrease in those in the G0/G1 and S phases. Flow cytometry analysis demonstrated a significant alteration in the distribution of MCF-7 cells in the cell cycle (Table 1, Fig. 3). The proportion of cells in the G1 phase and S phase was found higher as 32.53% and 19.77%, respectively, compared to the untreated control group which was found to be 24.87% in G1 phase and 15.27% in the S phase. Conversely, a decrease in the G2 phase population was observed upon SB5 treatment (31.25%) compared to the control, at 34.44% in the G2 phase (Fig. 4, Fig. 5). These results

Table 1 — *In vitro* anticancer activity of the synthesized compounds against human breast carcinoma cell line (MCF-7)

Compd	Cell Line	Compd	Cell Line
	MCF-7IC_{50} (µg/mL) Mean ± SEM		MCF-7IC_{50} (µg/mL) Mean ± SEM
SB-1	398.0 ± 0.06	**SB-5**	157.9 ± 0.12
SB-2	298.2 ± 0.06	**SB-6**	269.5 ± 0.09
SB-3	353.0 ± 0.05	**SB-7**	166.7 ± 0.09
SB-4	354.8 ± 0.08	–	–

50% Inhibitory concentrations (IC_{50}) in human breast carcinoma (MCF7), determined by the MTT assay after 24 h exposure. Data are quoted as mean ± standard deviation (SD) of four replicates (Fig. 2, Table 1). No activity was shown, by negative control 0.1% DMSO

imply that the treated compound causes a G1/S phase arrest, possibly through cyclin-dependent kinase inhibitors like p21 and p27, which are known to control the course of the cell cycle at the G1 checkpoint.

In silico studies / Computational studies

In silico ADMET Profiles

One important tool that helps pharmaceutical companies choose the right drug candidates before investing in extensive clinical trials is *in silico* ADMET prediction[56,57]. In this investigation, pharmacokinetics study was carried out employing pkCSM tool on the synthesized compounds to ascertain whether the compounds under investigation exhibit good ADMET profiles.

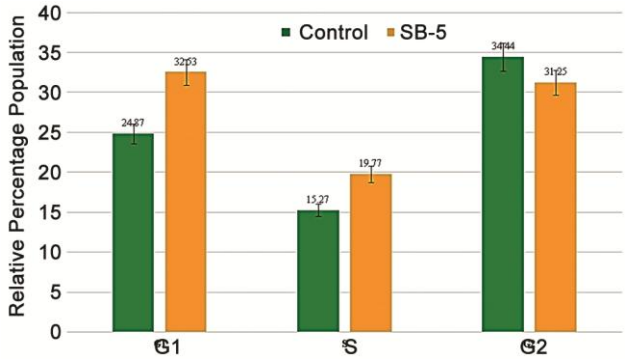

Fig. 3 — Graphical representation- Cell cycle analysis in MCF-7 cells treated with SB5

Drug bioavailability is influenced by water solubility and the ideal range is –5 to 0)[58]. Remarkably, all the synthesized compounds have good water solubility including reference drug. In order to assess the absorption and bioavailability of oral medications, the permeability of the colon cancer cell line (Caco-2)[59], is evaluated which found that all compounds have good permeability. Since, the intestinal system is where oral drugs are mostly absorbed, a medication absorption rate of less than 30% is considered inadequate in this context. Interestingly, newly synthesized compounds exhibited acceptable intestinal absorption due to their high rates value. A value > 0.5 for VDss indicates that the drug is well disseminated in the plasma, whereas a lower value (< –0.5) indicates that the medication's capacity to pass through the cell membrane is weak[60]. Here,

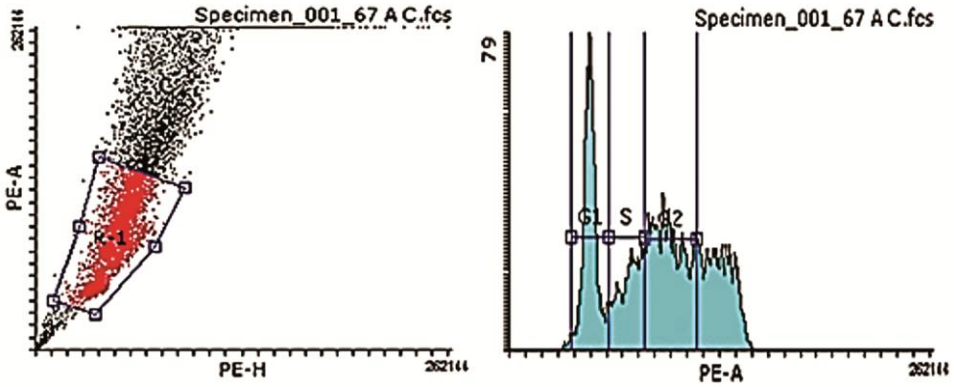

Fig. 4 — Flow cytometric analysis of MCF-7 cells exposed to the negative control

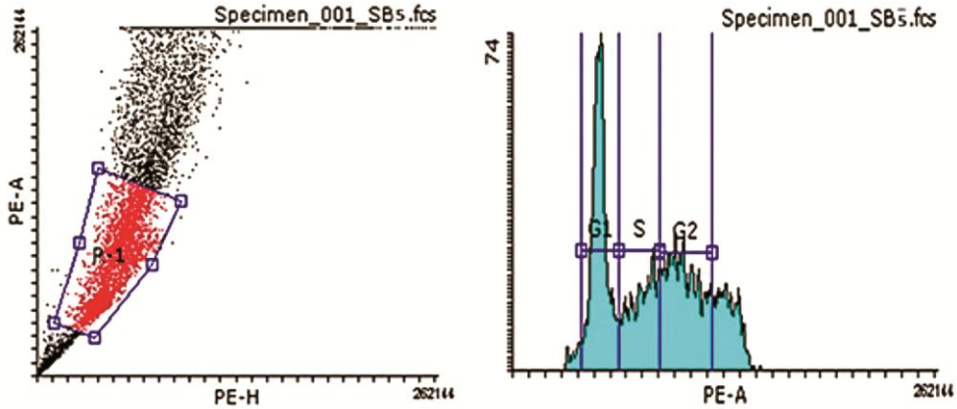

Fig. 5 — Flow cytometric analysis of MCF-7 cells treated with compound SB5

compounds SB1, SB2, SB3, and SB4 are moderately distributed while SB5, SB6, and SB7 are weakly distributed through the cell membrane. These synthesized compounds do not cross the BBB because compounds with a logBB ≤ 0.3 are not sufficiently distributed to the brain[61]. The drug metabolism is presented by CYPs, enzymes that convert drugs into more water-soluble forms for excretion during phase 1 metabolism. The effectiveness, bioavailablity, and possible toxicity of drugs are significantly influenced by these enzymes. The toxicity that attributes mutagenesity is represented by Ames toxicity and for drug that is toxic to liver is indicated by hepatotoxicity. The study showed compounds SB1, SB2, SB3, SB4, and SB5 do not indicates Ames toxicity while compounds SB3, SB4, SB5, SB6, and SB7 are not toxic to liver (Table 2). Additionally, a good total clearance number[58], suggests that the compounds have appropriate rate of excretion, which is advantageous to the body and means that the synthesized compounds will be able to clear as needed.

Molecular Docking

The principal factor for analysis of the molecular docking result involves examining binding energy, hydrogen bond interactions, and interacting residues. Since, the EGFR contributes a highly conserved catalytic loop, Asp 812- Asn 818, and a crucial regulatory activation loop, Asp 831- Val 852, to the protein, interactions with good binding affinity between synthesized compounds and these residues may restrict EGFR function.

SB1 interacted through H-bond with Arg 817, Asn 818, Asp 831, and Gly 697 and hydrophobic and van der Waals interactions with other important residues (Fig. 6) and binds with good binding energy of –10.2 kcal/mol. Here, the interactions between target protein

Table 2 — ADMET analysis of seven synthesized compounds along with reference drug (erlotinib)

	Parameters	SB1	SB2	SB3	SB4	SB5	SB6	SB7	Erlotinib
Absorption	Water Solubility	–3.514	–3.871	–3.633	–3.612	–2.631	–3.002	–2.064	–4.403
	Caco-2 Permeability (log Papp 10^{-6} cm/s)	0.231	0.732	0.09	0.917	0.029	0.029	0.079	1.24
	Intestinal Absorption (% absorbed)	78.69	88.65	86.78	88.73	71.75	82.08	81.93	95.55
Distribution	VDss (log L/kg)	0.058	–0.032	–0.075	0.127	–0.504	–0.777	–0.542	–0.053
	BBB permeability (log BB)	–1.283	–0.695	–0.988	–0.952	–1.014	–1.132	–0.508	–0.67
	CNS permeability (log PS)	–2.387	–2.191	–1.991	–1.935	–2.978	–3.418	–2.273	–3.384
Metabolism	CYP1A2	Yes	Yes	Yes	Yes	No	Yes	Yes	Yes
	CYP2C19	Yes	Yes	Yes	Yes	No	No	No	Yes
	CYP2C9	Yes	Yes	Yes	Yes	No	No	No	Yes
	CYP2D6	No	No	No	No	No	No	No	No
	CYP3A4	Yes	Yes	Yes	Yes	No	No	No	Yes
Excretion	Total clearance	0.897	1.154	0.882	–0.233	0.668	0.796	0.752	0.591
Toxicity	Ames Toxicity	No	No	No	No	No	Yes	Yes	No
	Hepatotoxicity	Yes	Yes	No	No	No	No	No	Yes

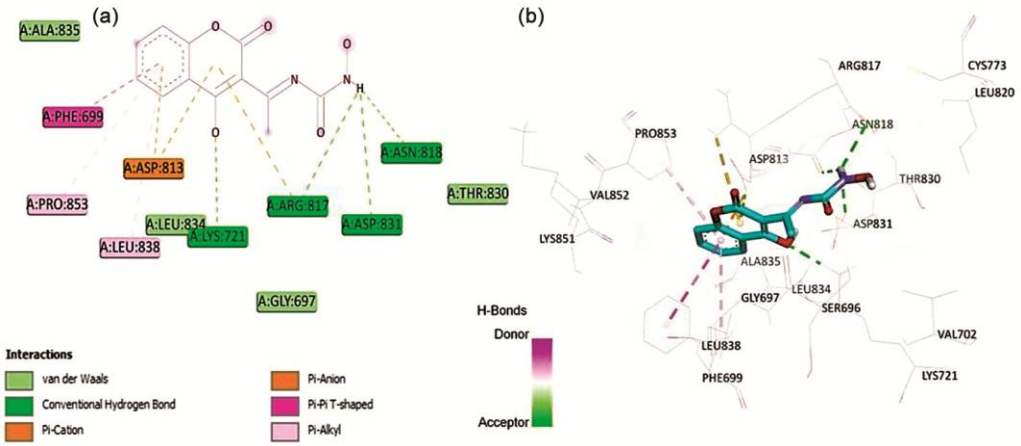

Fig. 6 — (a) and (b) represent 2D and 3D structures of complex of compound SB5 with EGFR

and compounds were facilitated by the presence of hydrogen bond donor group (-OH), hydrogen bond acceptors (O, and N), pi-bonds, and aromatic ring in the compounds. SB2 manifested the suitable binding energy of –9.9 kcal/mol while binding with target protein through H-bonds with Arg 817, Lys 721, and Pro 853 and other hydrophobic and van der Waals interactions. For the interactions of compounds, the ethereal oxygen, hydrogen bond acceptor (N and O-atoms), pi-bonds, and aromatic ring are responsible. Both compounds SB3 and SB4 showed binding energy of –9.5 kcal/mol with target protein that interacts with residues Lys 721 Arg 817, and Pro 853 through H-bonds interactions while other important residues interact through hydrophobic and van der Waals interactions. Compound SB5 and target protein bound with appreciable binding energy of –7.8 kcal/mol and interacted through H-bond, hydrophobic, and van der Waals interactions. Similarly, both SB6 and SB7 showed suitable binding energy of –7.8 kcal/mol with target protein and undergoes interactions with important amino acid residues. Compared to reference drug, erlotinib (Fig. 7), which binds target protein with binding energy of –7.3 kcal/mol, all the synthesized compounds displayed significant binding energies along with interactions with important residues of target protein (Table 3). Hence, the molecular docking study showed preferred binding interactions of synthetic compounds within binding pockets of EGFR as compared to the reference drug, erlotinib, which is an FDA-approved drug towards treating some types of non-small cell lung cancer and advanced pancreatic cancer, works as an inhibitor of EGFR (**Supplementary Information S36-S41**).

Density Functional Theory Analysis

Using the DFT method, semi-empirical molecular orbital calculations at the ground state were performed in order to better understand the energetic behavior of the synthesized compounds. This method investigates the reactivity of the compounds with target protein. Compounds with a lower band gap energy are usually more chemically reactive, have lower kinetic stability and more polarizable[62]. Based on the Pearson principle of maximum hardness, the

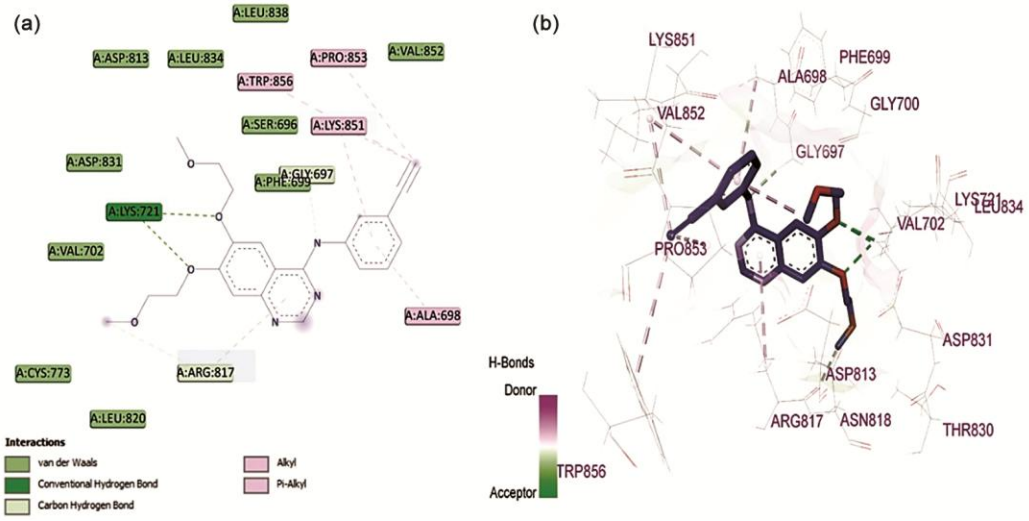

Fig. 7 — (c) and (d) represent 2D and 3D structures of complex of erlotinib with EGFR

Table 3 — Display of binding energies of synthesized compounds with various interacted residues of EGFR

Compd	Binding Energies (kcal/mol)	Binding interactions
SB1	–10.2	Arg 817, Asp 831, Asn 818, Gly 697, Lys 721, Lys 851, Trp 856, Pro 853, Val 702
SB2	–9.9	Arg 817, Lys 721, Pro 853, Trp 856, Val 702, Lys 851
SB3	–9.5	Lys 721, Arg 817, Pro 853, Val 702, Trp 856, Lys 851
SB4	–9.5	Lys 721, Arg 817, Pro 853, Val 702, Trp 856, Lys 851
SB5	–7.9	Lys 721, Arg 817, Asn 818,Asp 831, Phe 699, Pro 853, Leu 838, Asp 813
SB6	–7.8	Arg 817, Pro 853, Thr 701, Asp 813, Lys 721, Gly 697, Asp 831, Ser 696
SB7	–7.8	Arg 812, Tyr 867, Asp 813, Leu 838
Erlotinib	–7.3	Arg 817, Gly 697, Lys 721, Lys 851, Trp 856, Pro 853, Ala 698

more reactive compounds have a higher softness value and a lower hardness[63]. The more chemically reactive compounds are with the target protein because they function well as electrophiles, the higher electronegativity value and electrophilicity indices[64].

According to DFT study analysis, all synthesized compounds (Fig. 8) were determined to have lower band gap energy compared to the reference drug, erlotinib (4.25 eV) which represents high reactivity of the synthesized compounds with target protein. Additionally, the global softness, global hardness, chemical potential, electron affinity, ionization potential, electronegativity, and electrophilicity–all of which are reactivity related–provide evidence (Table 4) for the good efficacy of these compounds against EGFR.

An analysis method for projecting the electrostatic potential onto the isoelectronic density surface and determining reactive site information is to plot the molecular electrostatic potential (MEP) surface in three dimensions. MEP maps of the compounds were developed by the study in order to identify the electron-rich and electron-deficient locations inside the compounds[65]. Gaussian 09 was employed to obtain MEP maps from DFT (B3LYP/6-31G') calculations, and GaussView 6.0 is used to visualize. The MEP map is depicted using the color scheme. The blue area in the illustration represents the positive region, which is associated with a nucleophilic attack. Conversely, the yellow color indicates a small area that is slightly electron-rich, and red color indicates a negative zone that is indicator of an electrophilic attack. And the green coloring denotes the compound's zero potential areas.

According to the study, positive charges were displayed by hydrogen atoms in their bonds with

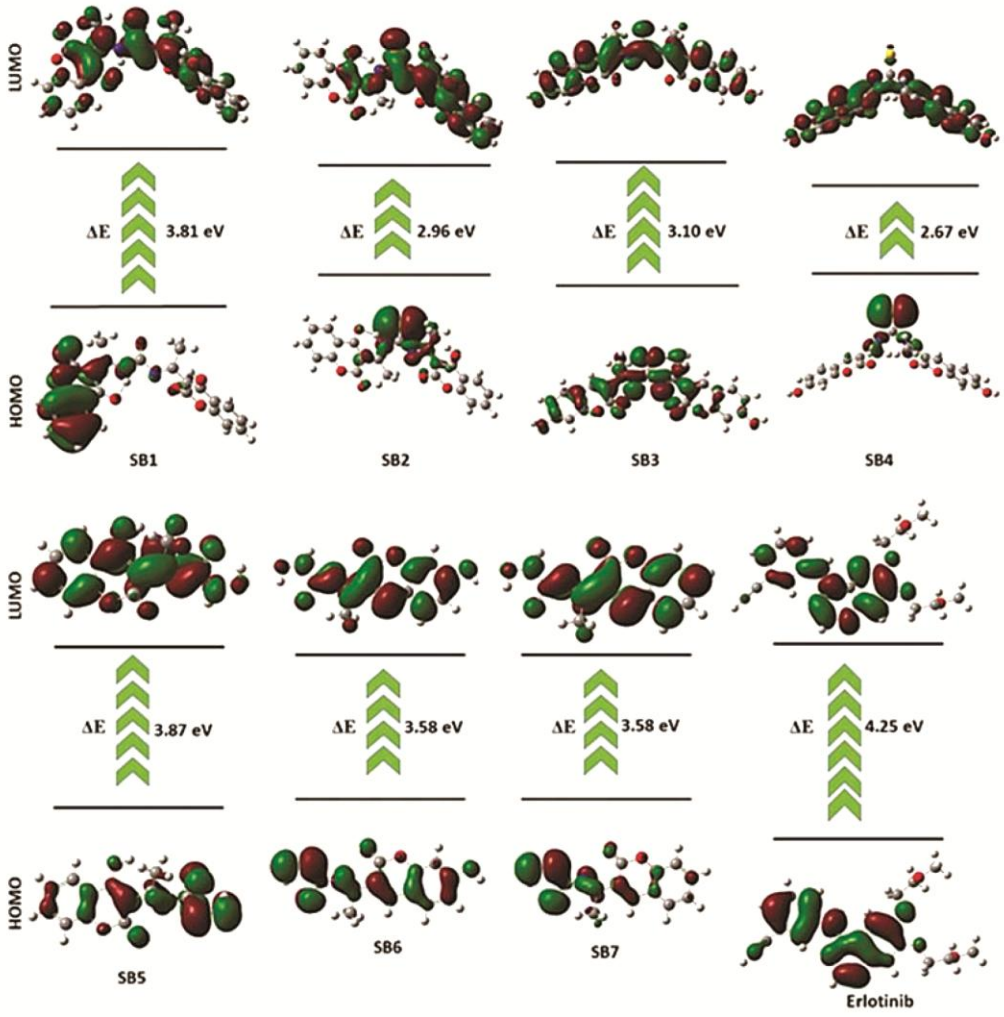

Fig. 8 — Band gap energy of the compounds SB1-SB7, including erlotinib

Table 4 — Density function theory analysis results in terms of the chemical reactivity descriptors

Parameters	**SB1**	**SB2**	**SB3**	**SB4**	**SB5**	**SB6**	**SB7**	Erlotinib
E_{LUMO} (eV)	–2.93	–3.10	–2.56	–2.51	–2.51	–2.67	–2.77	–1.26
E_{HOMO} (eV)	–6.74	–6.06	–5.66	–5.18	–6.48	–6.25	–6.35	–5.51
Band energy gap (ΔE) (eV)	3.81	2.96	3.1	2.67	3.97	3.58	3.58	4.25
Ionization potential (I) (eV)	6.74	6.06	5.66	5.18	6.48	6.25	6.35	5.51
Electron affinity (A) (eV)	2.93	3.10	2.56	2.51	2.51	2.67	2.77	1.26
Global hardness (η) (eV)	1.905	1.48	1.55	1.335	1.985	1.79	1.79	2.125
Global softness (S) (eV^{-1})	0.52	0.68	0.65	0.75	0.50	0.56	0.56	0.47
Electronegativity (χ) (eV)	4.84	4.58	4.11	3.85	4.50	4.46	4.56	3.39
Chemical potential (μ) (eV)	–4.84	–4.58	–4.11	–3.85	–4.50	–4.46	–4.56	–3.39
Electrophilicity index (ω) (eV)	6.15	7.09	5.44	5.55	5.10	5.55	4.89	2.70

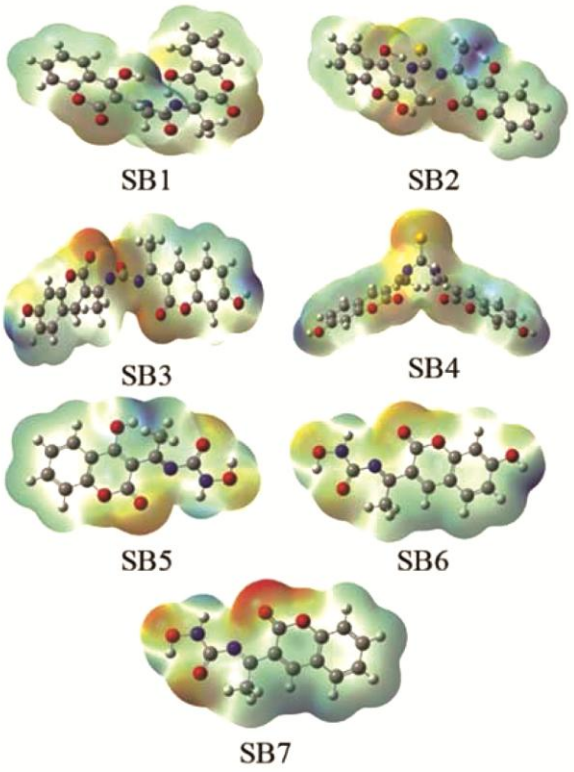

Fig. 9 — Molecular electrostatic potential maps of the compounds SB1-SB7

oxygen and nitrogen atoms, whereas negative charges were displayed by oxygen and nitrogen atoms. As shown in Fig. 9, the red area of the MEP map depicts the electron-rich center, suggests a hydrogen bond interaction between the oxygen atom of synthesized compounds and hydrogen of the hydroxyl and amine group of important amino acid residues of EGFR. In order to support the results obtained from molecular docking, this study further examines the binding patterns and molecular interactions between synthesized compounds and target protein.

Conclusion

With IC_{50} values ranging 157.9 ± 0.12—398.0 ± 0.06 µg/mL against the tested MCF-7 cancer cell line, these synthesized compounds demonstrated well to moderate cytotoxicity. The cell cycle analysis of the compound, SB5 exhibited lower proportion of cells in G2 phase, higher proportion of cells in G1 and S phases. The treated compound induced cell cycle arrest at G1/S phase. Schiff bases have high negative binding-free energy values against EGFR, according to the docking analysis which indicates that their binding affinities are favorable, and their binding interactions are facilitated by the hydrogen bonds at the binding sites. The results imply that these substances might be the focus of more research as potential new anticancer drugs.

Supplementary Information

Supplementary information is available in the website http://nopr.niscpr.res.in/handle/123456789/58776.

Acknowledgement

We sincerely acknowledge Aakaar Biotechnologies Pvt. Ltd. Lucknow, Uttar Pradesh, India for anticancer screening. Nepal Academy of Science and Technology, Lalitpur, Nepal for UV and FT-IR data, Indian Institute of Technology (IIT) Madras, India, for the CHNS, and HR-MS Esi data, Indian Institute of Science (IISc), Bangalore, India, for NMR data.

Conflicts of Interest

The authors declare no conflict of interest.

Funding statement

This research was not funded by any specific grants from public, commercial, or non-profit funding agencies.

Author contributions: CRediT

Anand Kumar Yadav: Writing original draft, Methodology, Synthesis and Characterization of Compounds. Manoj Silwal: Computational study. Neeta Singh: Formal analysis; Achyut Adhikari: Conceptualization; Paras Nath Yadav: Project administration, Supervision.

References

1 Önder A, *Stud Nat Prod Chem*, 64 (2020) 85.
2 Ortega M A, Fraile-Martínez O, Asúnsolo Á, Buján J, García-Honduvilla N & Coca S, *J Oncol*, 2020 (2020) 9258396.
3 Zhang L & Xu Z, *Eur J Med Chem*, 181 (2019) 111587.
4 Govindaiah P, Dumala N, Grover P & Jaya Prakash M, *Med Chem Lett*, 29 (2019) 1824.
5 Herrera-R A, Naranjo T W, Maldonado M E, Moreno-Q G, Yepes A & Cardona-G W, *Med Chem Res*, 29 (2020) 377.
6 Vaseghi S, Yousefi M, Shokrzadeh M, Hossaini Z, Hosseini-khah Z & Emami S, *Mol Diversity*, 25 (2021) 1011.
7 Durgapal S D, Soni R, Umar S, Suresh B & Soman S S, *ChemistrySelect*, 2 (2017) 147.
8 Fois B, Distinto S, Meleddu R, Deplano S, Maccioni E, Floris C, Rosa A, Nieddu M, Caboni P, Sissi C, Angeli A, Supuran C T & Cottiglia F, *J Enzyme Inhibit MedChem*, 35 (2020) 539.
9 Hussein D M, Al-Juboory S B & Razzak Mahmood Kubba A A, *Orient J Chem*, 33 (2017) 768.
10 Verma S K, Savani C & Singh V K, *ChemistrySelect*, 4 (2019) 14244.
11 Pereira T M, Franco D P, Vitorio F & Kummerle A E, *Curr Top Med Chem*, 18 (2018) 124.
12 Yadav A K, Maharjan R S, & Yadav P N, *Eur J Med Chem*, 267 (2024) 116179.
13 Shrestha R M, Mahiya K, Shrestha A, Mohanty S R, Yadav S K & Yadav P N, *Inorg Chem Commun*, 161 (2024) 112142.
14 Yadav A K, Singh N, Silwal M, Adhikari A & Yadav P N, *Results Chem*, 11 (2024) 101794.
15 15 Karakus G, Kaplan Can H & Sahin Yaglioglu A, *J Mol Struct*, 1210 (2020) 127989.
16 Shrestha R M, Mahiya K, Shrestha A & Ranjan S, Yadav P N, *J Mol Struct*, 1299 (2023) 136945. 17.
17 Listro R, Rossino G, Piaggi F, Sonekan F F, Rossi D, Linciano P & Collina S, *Front Chem*, 10 (2022) 1.
18 Agili F A, *Chemistry (Switzerland)*, 6 (2024) 435.
19 Stadlbauer W & Hojas G, *J Heterocycle Chem*, 41 (2004) 681.
20 Bahron H, Khaidir S S, Tajuddin A M, Ramasamy K & Yamin B M, *Polyhedron*, 161 (2019) 84.
21 Patil P, Betageri V S, Kinnal S M & Latha M S, *IOP Conf Ser: Mater Sci Eng*, 925 (2020) 012052.
22 Hamid S J & Salih T, *Drug Des, Dev Ther*, 16 (2022) 2275.
23 Goodsell D S & Olson A J, *Proteins: Struct, Funct, Bioinf*, 8 (1990) 195.
24 Shrestha A, Upadhyaya S R, Raut B K, Bhattarai S, Sharma K R, Parajuli N, Sohng J K & Regmi B P, *Processes*, 12 (2024) 230.
25 Abkari A. Chaabane I & Guidara K, *Physica E: Low-Dimensional Systems and Nanostructures*, 81 (2016) 136.
26 Lin L, Sun S & Yu Q, *Spectrochim Acta - Part B At Spectrosc*, 217 (2024) 106959.
27 Lungu L, Ciocarlan A, Barba A, Shova S, Pogrebnoi S, Mangalagiu I, Moldoveanu C, Vornicu N, D'Ambrosio M, Babak M V, Arion V B & Aricu A, *Chem. Heterocycl. Compd*, 55 (2019) 716
28 Šarkanj B, Molnar M, Čačić M & Gille L, *Food Chem*, 139 (2013) 488.
29 Indira S, Vinoth G, Bharathi M & Shanmuga Bharathi K, *J Mol Struct*, 1198 (2019) 126886.
30 Vekariya R H, Patel K D, Rajani D P, Rajani S D & Patel H D, *J Assoc Univ Basic Appl Sci*, 23 (2017) 10.
31 Toan V N & Thanh N D, *Med Chem Res*, 30 (2021) 1868.
32 Arjunan V, Sakiladevi S, Marchewka M K & Mohan S, *Spectrochim Acta - Part A: Molecular and Biomolecular Spectroscopy*, 109 (2013) 79. https://doi.org/10.1016/j.saa.2013.01.100
33 Thanh N D, Van H T K & Thu T T, *Thu J Carbohydr Chem*, 34 (2015) 514.
34 Aroua L M, Al-Hakimi A N, Abdulghani M A M & Alhag S K, *Arabian J Chem*, 15 (2022) 103986.
35 Qi F, Qi Q, Song J & Huang J, *Chem Biodiversity*, 18 (2021) 1.
36 Benazzouz-Touami A, Hikem-Oukacha D, Lamara K O, Halit S, Terrachet-Bouaziz S & Makhloufi-Chebli M, *Chem Data Collect*, 36 (2021) 100792.
37 Low M L, Paulus G, Dorlet P, Guillot R, Rosli R, Delsuc N, Crouse K A & Policar C, *BioMetals*, 28 (2015) 553.
38 Alwan W M, *J Phy ConferenceSeries*, 1003 (2018) 012017.
39 Branca C, D'Angelo G, Crupi C, Khouzami K, Rifici S, Ruello G & Wanderlingh U, *Polymer*, 99 (2016) 614.
40 Hejchman E, Kruszewska H, Maciejewska D, Sowirka-Taciak B, Tomczyk M, Sztokfisz-Ignasiak A, Jankowski J & Młynarczuk-Biały I, *Monatshefte Fur Chemie*, 150 (2019) 255.
41 Abou-Melha K S, *J Coord Chem*, 61 (2008) 2053.
42 Sanmartin J, Bermejo M R, Garcia-Deibe A M, Rivas I M & Fernândez A R, *J Chem Soc Trans*, 22 (2000) 4174.
43 Tantaru G, Poiata A, Bibire N, Panainte A D, Apostu M & Vieriu M, *Revista de Chimie*, 68 (2017) 586.
44 Braga T C, Silva M M, Nascimento E O O, da Silva D E C, de Freitas R Y, Mandal M, de Souza A Z, Tasca Góis Ruiz A L, de Carvalho E J, Martins F T, Figueiredo I M, de Aquino M T, Moreira da Silva C, Mandal B, Brahmachari G, Caldas Santos J C & de Fátima Â, *Eur J Chem Rep*, 4 (2022) 100030.
45 Pangal A, Shaikh J A, Gazge M, Mane V & Ahmed K, *Int Res J Pharm*, 4 (2013) 108.
46 Rahman F S A, Yusufzai S K, Osman H & Mohamad D, *J Phys Sci*, 27 (2016) 77.
47 Ren S, Wang R, Komatsu K, Bonaz-Krause P, Zyrianov Y, McKenna C E, Csipke C, Tokes Z A & Lien E J, *J Med Chem*, 45 (2002) 410.
48 El-Ansary A L, Moustafa H, Abdel-Kader N S & Farghaly A M, *Appl Organomet Chem*, 33 (2019) 1.
49 Issa R M, Khedr A M & Rizk H, *J Chinese Chem Soc*, 55 (2008) 875.
50 Sidir Y G, Sidir I, Berber H & Türkoğlu G, *J Mol Liq*, 204 (2015) 33.
51 Fotakis G & Timbrell J A, *Toxicol Lett*, 160 (2006) 171.
52 Miri R, Nejati M, Saso L, Khakdan F, Parshad B, Mathur D, Parmar V S, Bracke M E, Prasad A K, Sharma S K & Firuzi O, *Pharm Biol*, 54 (2016) 105.

53 Khan F, Ahmed F, Pushparaj P N, Abuzenadah A, Kumosani T, Barbour E, Al Qahtani M & Gauthaman K, *PLoS ONE*, 11 (2016) 1.
54 Dalton S, *Trends in cell biology*, *25* (2015) 592.
55 Yao Y, Zhang B, Chen H, Chen N, Liu L, Yashan W, Li C & Zheng Q, *Journal of Pharmacy and Pharmacology*, 64 (2012) 101.
56 Alqahtani S, *Expert Opin Drug Metab Toxicol*, 13 (2017) 1147.
57 Chaudhary U, Kumar P, Sharma P, Chikara A, Barua A, Mahiya K, Adhikari Subin J, Yadav P N & Pokharel Y R, *Bioorg Chem*, 153 (2024) 107872.
58 Putri S A, Julaeha E, Kagawa N & Kurnia D, *Wiley E-J Chem*, 2024 (2024) 3696250.
59 Lagorce D, Douguet D, Miteva M A & Villoutreix B O, *Sci Rep*, 7 (2017) 1.
60 El-Shamy N T, Alkaoud A M, Hussein R K, Ibrahim M A, Alhamzani A G & Abou-Krisha M M, *Molecules*, 27 (2022) 1.
61 Muehlbacher M, Spitzer G M, Liedl K R & Kornhuber J, *J Comput-Aided Mol Des*, 25 (2011) 1095
62 Huang Y, Rong C, Zhang R & Liu S, *J Mol Model*, 23 (2017) 1.
63 Kumar C B P, Raghu M S, Prasad K N N, Chandrasekhar S, Jayanna B K, Alharthi F A, Prashanth M K & Kumar K Y, *New J Chem*, 45 (2021) 403.
64 Xu H, Tu X, Fan G, Wang Q, Wang X & Chu X, *J Mol Liq*, 318 (2020) 114315.
65 Uzun S, Esen Z, Koç E, Usta N C & Ceylan M, *J Mol Struct*, 1178 (2019) 450.